Challenging Glass Conference Proceedings – Volume 10 – June 2026 – Louter, Bos & Belis (Eds.)
International Conference on the Architectural and Structural Application of Glass
Challenging Glass Conference 10 – 15-17 June 2026 – TU Delft – The Netherlands

Seismic Performance of Point-Fixed Glass Façade Systems

Seyed Amin Hosseini [a], Sandra Jordão [a], Carlos Rebelo [a], Chiara Bedon [b], Rohola Rahnavard [a]

a University of Coimbra, ISISE, Department of Civil Engineering, Portugal
s.amin9068@gmail.com, sjordao@dec.uc.pt, crebelo@dec.uc.pt, rahnavard1990@gmail.com
b University of Trieste, Department of Engineering and Architecture, Italy
chiara.bedon@dia.units.it

Abstract

Point-fixed glass façade systems (PFGFSs) are widely used as modern building envelopes. This type of façade is particularly susceptible to seismic action; however, its seismic performance hasn't been sufficiently quantified. To address this challenge, the seismic behaviour of a 3D steel moment-resisting frame (SMRF) with PFGFS was evaluated. The model includes the SMRF, laminated glass panels (LGP), spider arms, and substructure. The numerical model was analysed for 15 pairs of earthquake acceleration spectra at three levels of intensity. The results clearly indicate that the PFGFS experiences substantially higher seismic demands than the main structural frame. Specifically, inter-storey drift ratios (IDRs) and peak floor accelerations (PFA) values in the façade system were up to 70% and 80% greater than those of the SMRF, respectively, particularly at upper storeys and under Near Collapse (NeC) level earthquakes. These results indicate that the PFGFS does not simply follow the response of the primary structural frame. Instead, the façade system experiences amplified dynamic effects under seismic loading. Therefore, façade systems require independent seismic assessment rather than relying solely on structural frame response.

Keywords

Glass façade, numerical model, point-fixed glass façade, seismic behaviour

Article Information

- Digital Object Identifier (DOI): 10.47982/cgc.10.749
- Published by Challenging Glass, on behalf of the author(s), at Stichting OpenAccess.
- Published as part of the peer-reviewed Challenging Glass Conference Proceedings, Volume 10, June 2026, 10.47982/cgc.10
- Editors: Christian Louter, Freek Bos & Jan Belis

1. Introduction

Glass Façade Systems (GFSs) have become a common feature in modern constructions, offering significant advantages in terms of architectural, aesthetic, thermal and lighting aspects (Takeuchi et al., 2006, 2009). Nevertheless, due to the brittle behaviour and relatively low tensile strength of glass panels, they are the most vulnerable components of buildings (Bedon et al., 2018).

Based on connection details, the GFSs are categorised into two groups of façade systems: Framed Glass Façade Systems (FGFSs) and Point Fixed Glass Façade Systems (PFGFSs), as shown in Fig. 1 (S. A. Hosseini et al., 2022; Inca-Cabrera et al., 2025). The main difference in these systems lies in how the glass panels are supported. FGFSs use continuous aluminium framing systems to attach the glass to the main structure, whereas metal spider arms are the typical connections in the PFGFSs (Sivanerupan et al., 2014).

Fig. 1: Glass façade systems: FGFSs (left) and PFGFS (right).

The seismic performance of GFSs highlights the important safety and economic concerns (Pantelides et al., 1996). First, the failure of glass panels during an earthquake may endanger occupants and pedestrians by causing broken glass to fall. Because of the glass materials' brittle behaviour, damage to the façade can occur suddenly and without significant warning. Therefore, GFSs require a higher reliability level than many other non-structural components (Code, 2014). Second, façade damage can result in substantial economic losses, including repair costs and service interruption of the building during rehabilitation works (Pantelides et al., 1996).

Earthquake-induced damage to non-structural components generally occurs through several mechanisms: A. Inertial or vibration effects, B. Damage to the connection between non-structural and main structure due to structural displacements, C. Pounding or separation between two individual buildings causes damage that appears in non-structural components between the structures, and D. interaction between two separate non-structural systems (FEMA E-74, 2012). For example, during the Alaska earthquake (1964), two people died due to glass failure (Pantelides et al., 1996). Severe glass failure caused a reduction, up to 50%, in the serviceability of Sea-Tac Airport (2001 Nisqually, Washington) (Filiatrault et al., 2001). Surveys after the 2011 Christchurch Earthquake showed that approximately 50% of GFSs had glass damage, and 39% had a falling-glass hazard. In this event, heavy damage to PFGFSs was reported. Fig. 2 shows the damage to PFGFSs during the 2011 Christchurch Earthquake. This damage was likely due to stress concentration around the spider where it was connected to the glass panes (Baird et al., 2011). Also, several other GFS failures were reported after moderate to severe earthquakes worldwide (Baird et al., 2014; Behr et al., 1995; Fierro et al., 2011; M. Hosseini, 2005; Miranda et al., 2012).

Fig. 2: Seismic damage to PFGFSs (Baird et al., 2011).

The objective of this paper is to evaluate the seismic behaviour of a building with PFGFSs. A five-storey steel moment-resistant frame (SMRF) incorporating PFGFSs is numerically analysed. The building is subjected to 15 pairs of far-field earthquakes, scaled according to Eurocode 8 Part 1 (EC 8-1). The seismic behaviour of SMRF and PFGFS is evaluated using global and local engineering demand parameters (EDPs). The inter-story drift ratios (IDRs) and peak floor accelerations (PFAs) are used to assess global and plastic deformation in connections used as local EDPs.

2. Case study building and selected earthquakes

2.1. Case study

A five-story SMRF office building incorporating PFGFS was selected as the case study building. The buildings fall under Category B according to Eurocode 1 part 1, and they were designed according to the European standards. The height of the first story was 4.0 m, while the remaining storeys were 3.5 m high. The structural layout consisted of 5 bays in the X-direction and 3 bays in the Y-direction, giving overall plan dimensions of 30 m × 21 m.

The building was assumed to be in a high-seismic hazard region. The seismic actions were defined according to EC8-1 for the soil Type C and a Type 1 spectrum, with a reference peak ground acceleration of a_{gR} = 0.25g (where g is the acceleration of gravity). A behaviour factor (q) of 6.5 was adopted for SMRFs with a high ductility class (HDC). The design was controlled by limiting the IDR to 1.00% at the Damage limitation state.

Columns were designed using square hollow sections (SHS), while beams were assigned IPE profiles. All beams and columns are made of S355 steel. All column bases and beam-column joints were assumed to be rigid, and rigid diaphragm behaviour was considered at each floor. Fig. 3 illustrates the plan and elevation views of the building. The detailed information regarding design considerations is presented in reference (S. A. Hosseini et al., 2024).

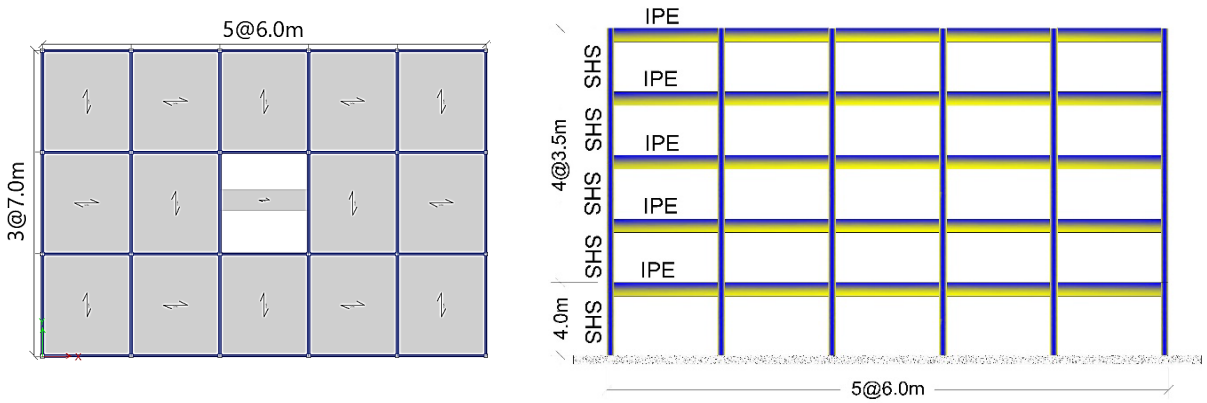

Fig. 3: Plan and elevation view of index buildings.

2.2. Numerical model

The three-dimensional nonlinear finite element model was developed in Abaqus software. All beams and columns were simulated using beam elements with cross-sections similar to the design sections. The gravity load was applied as a point mass at the top flange of the beams. The model consists of 11,176 beam elements with an average length of 150 mm. The steel material was represented using an elastic-plastic model. The material characteristics are presented in Table 1.

The PFGFSs were modelled by explicitly representing the laminated glass panels (LGPs), spider arms, façade substructure, and their interaction with the main structural frame. In total, 90 LGPs were arranged in a 10 × 9 configuration. Each LGP measures 2090 × 1990 mm and has a total thickness of 17.52 mm, consisting of two tempered glass plies bonded by a 1.52 mm EVASAFE interlayer. The inner and outer glass plies are 6 mm and 10 mm thick, respectively. A 10mm gap separates adjacent panels.

All LGPs are connected to the façade substructure through stainless steel spider arms. The façade substructure comprises circular hollow-section (CHS) steel members, with columns of 60.30 × 5 mm and beams of 139.7 × 8 mm cross-section. Fig. 4 illustrates the main structure, façade substructure and the connection zone.

Each LGP uses a composite shell element, S4R, with three plies (Glass–EVASAFE–Glass) and three integration points per ply. Per panel, 512 S4R elements (linear quadrilaterals) and 16 S3 elements (linear triangles) are employed. To capture stress concentrations around the bolt holes, the mesh density is refined locally near the glass–spider connection zones. The columns and beams of the façade substructure and the SMRF are modelled using B31 beam elements. The substructure is connected to the main structure using square hollow-section (SHS) members at each storey level. These members were modelled using B31 beam elements.

The spider arm assembly is divided into two functional components: (i) spider support, modelled using beam elements (B31); and (ii) spider bridge connection, linking the support to the LGP hole using connector elements. The connector system consisted of two components: (i) Cartesian + Align connector, positioned between the spider support and the glass hole; and (ii) Join-Rotation connector, assigned to the link between the spider arm and the edge of the LGP hole to account for the 8 degrees of freedom associated with in-plane rotation.

The façade substructure and main structure are made of carbon steel, while stainless steel is used for the spider arms. The mechanical characterisation of all materials is summarised in Table 1.

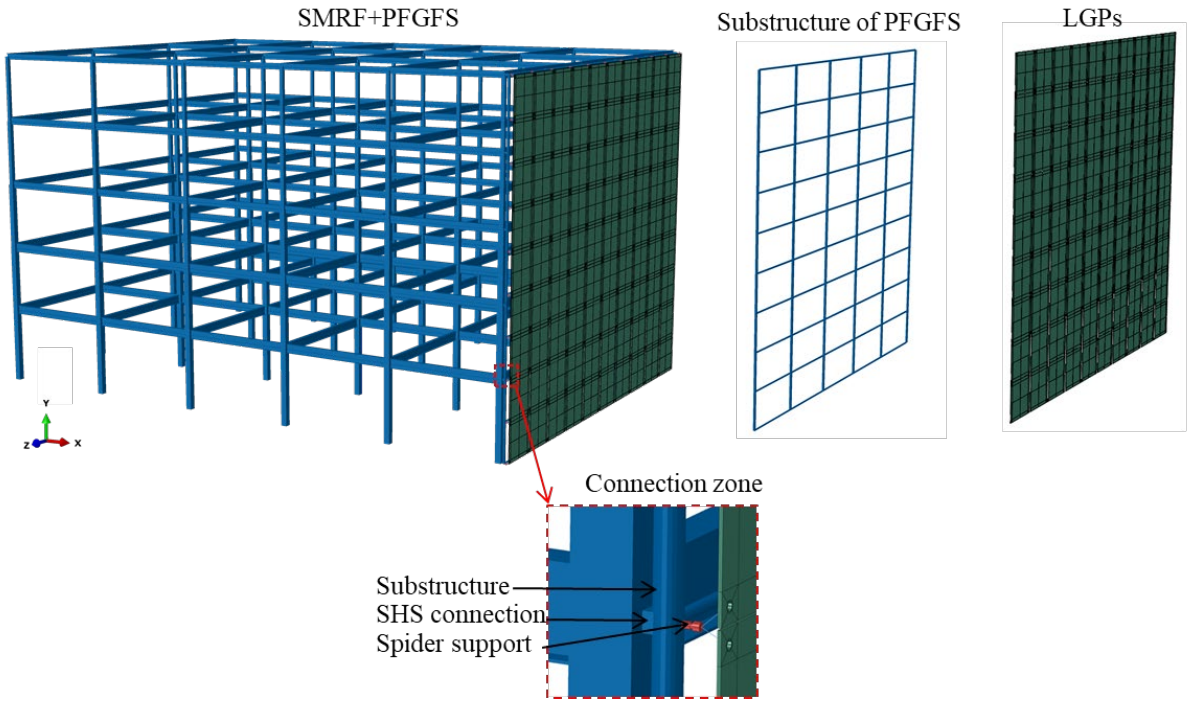

Fig. 4: Numerical model of SMRF with PFGFS.

Table 1: Material characterisation.

Material	Density (ton/mm^3)	E (GPa)	$\nu(-)$	f_y (MPa)	F_u (MPa)	ε_u $(-)$
Glass	2.6E-09	70	0.23			
EVACES	1.07E-09	0.010	0.49			
Stainless steel	7.85E-09	202.04	0.30	208.37	757.01	0.36
Steel S355	7.85E-09	202.47	0.30	427.19	590.18	0.09

E: Modulus of elasticity; ν: Poisson´s ratio; f_y: Yield stress; f_u: Ultimate stress; ε_u: Ultimate strain

In this study, 15 pairs of far-field earthquakes were selected from the PEER Strong Motion Database (PEER). Referring to EC8, the selected ground motion records were scaled to three seismic intensity levels, corresponding to Damage Limitation (DaL), Significant Damage (SiD), and Near Collapse (NeC) states (S. A. Hosseini et al., 2025). The 0.2T and 2.0T are the ranges of spectrum considered for the matching process (T is the SMRF fundamental period). The spectrum of the selected earthquakes and the comparisons with the design spectrum of EC8-1 are presented in Fig. 5.

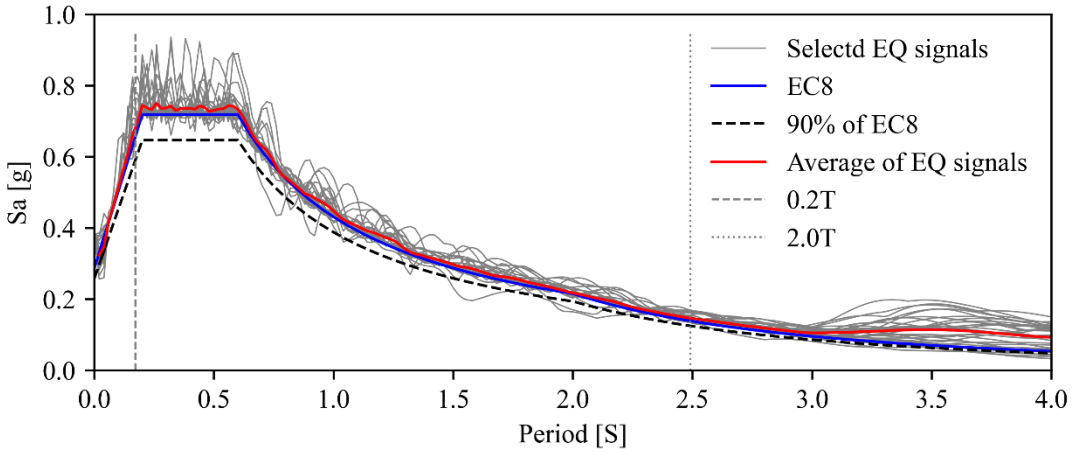

Fig. 5: Elastic spectrum of selected earthquake events.

The results of the numerical simulations were assessed for both global and local levels. IDR and PFA were evaluated for both the main SMRF and PFGFS. Furthermore, the plastic behaviour of the spider arm connectors was evaluated, given their importance in maintaining the integrity during strong ground motions.

3. Seismic response of PFGFS

3.1. Global seismic response

Fig. 6 illustrates the variation of IDR and PFA along the building height for both SMRF and PFGFS. The vertical axis represents the relative height (z/h), where z is the height of the measured storey, and h is the total height.

Across all seismic intensity levels, the PFGFS consistently experiences higher demands than the SMRF. For both systems, the peak responses occur at the roof level (S5), indicating amplification effects towards the upper storeys. In terms of IDR, the PFGFS shows substantially larger values. The IDR demand in the PFGFS is around 50% higher than that of the SMRF at the DaL and SiD levels, and increases to nearly 70% at the NeC level.

The results demonstrate that, across all earthquake intensity levels, the seismic demands on the PFGFS are significantly higher than those on the SMRF. The maximum global responses for both systems occur at the roof level (Storey 5, S5). PFAs follow the same patterns. The highest PFA values are recorded at the roof level for all intensities. At the NeC level, the PFA of PFGFS reaches 1.87g, which is approximately 80% higher than that of the SMRF. Even at lower intensity levels, the façade PFA exceeds the structural response by 38% (DaL) and 46% (SiD).

These findings demonstrate that the PFGFS undergoes notable dynamic amplification, particularly in the upper storeys and under strong ground motions. The behavior conforms that PFGFS cannot be assumed to follow the structural responses directly and should be evaluated independently in seismic design.

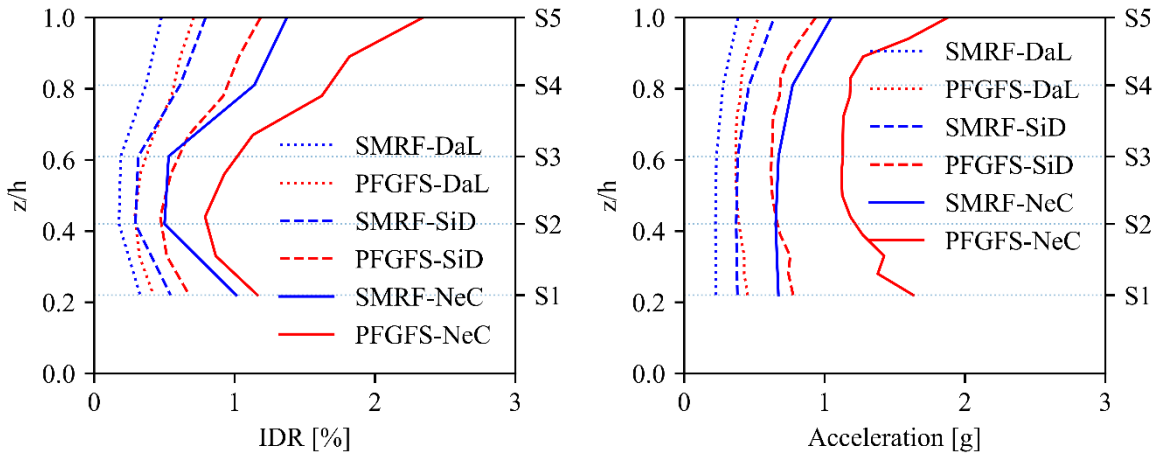

Fig. 6: Global response of SMRF and PFGFS (IDR and Acceleration).

3.2. Local behaviour of spider arms

To better understand local damage mechanisms, the plastic behaviour of the spider arm connectors was examined. These connectors are critical components of the PFGFS's load-transfer mechanism. The equivalent plastic motion (CUPEQ) was used as a quantitative measure of the deformation of connector. CUPEQ stands for Connector Equivalent Plastic Relative Displacements/Rotations corresponding to an Abaqus output parameter for the lamped assessment of accumulated plasticity at a ductile connector during transient non-linear analysis.

At the DaL level, the maximum CUPEQ is approximately 20 mm; however, when the structures are subjected to NeC excitation, the maximum value increases significantly to about 150 mm. This sharp increase highlights the strong nonlinear responses of the connectors under severe seismic actions.

Fig. 7 presents the statistical distribution of maximum CUPEQ values for all 15 ground motions using box plots. The data is grouped by storey location (Ground to S5). The box represents the interquartile range; a horizontal red line indicates the median; and a green marker shows the mean.

At storey 5, the median values rise from 6.45 mm (DaL) to 31.09 mm (SiD) and reach 92.53 mm (NeC). Connectors at the upper storeys, particularly near story 4, experienced the highest deformation demands. This can be attributed to acceleration and drift amplifications at higher elevations. A CUPEC threshold of 3.0 mm, corresponding to the connector yielding displacement, was defined. While only some connectors exceed this limit under DaL at higher storeys, most connectors surpass it under SiD and NeC, indicating significant plastic behaviour.

4. Conclusion

This research evaluated the global and local seismic responses of a five-storey SMRF with PFGFS using nonlinear finite element analysis. The results consistently showed that the PFGFS is subjected to significantly greater demands than the primary structure. IDR and PFA values in the PFGFS exceeded those of SMRF by up to 70% and 80%, respectively, particularly at higher stories and under NeC-level earthquakes. These results show that the PFGFS do not simply follow structural responses but may experience amplified dynamic effects that warrant independent consideration.

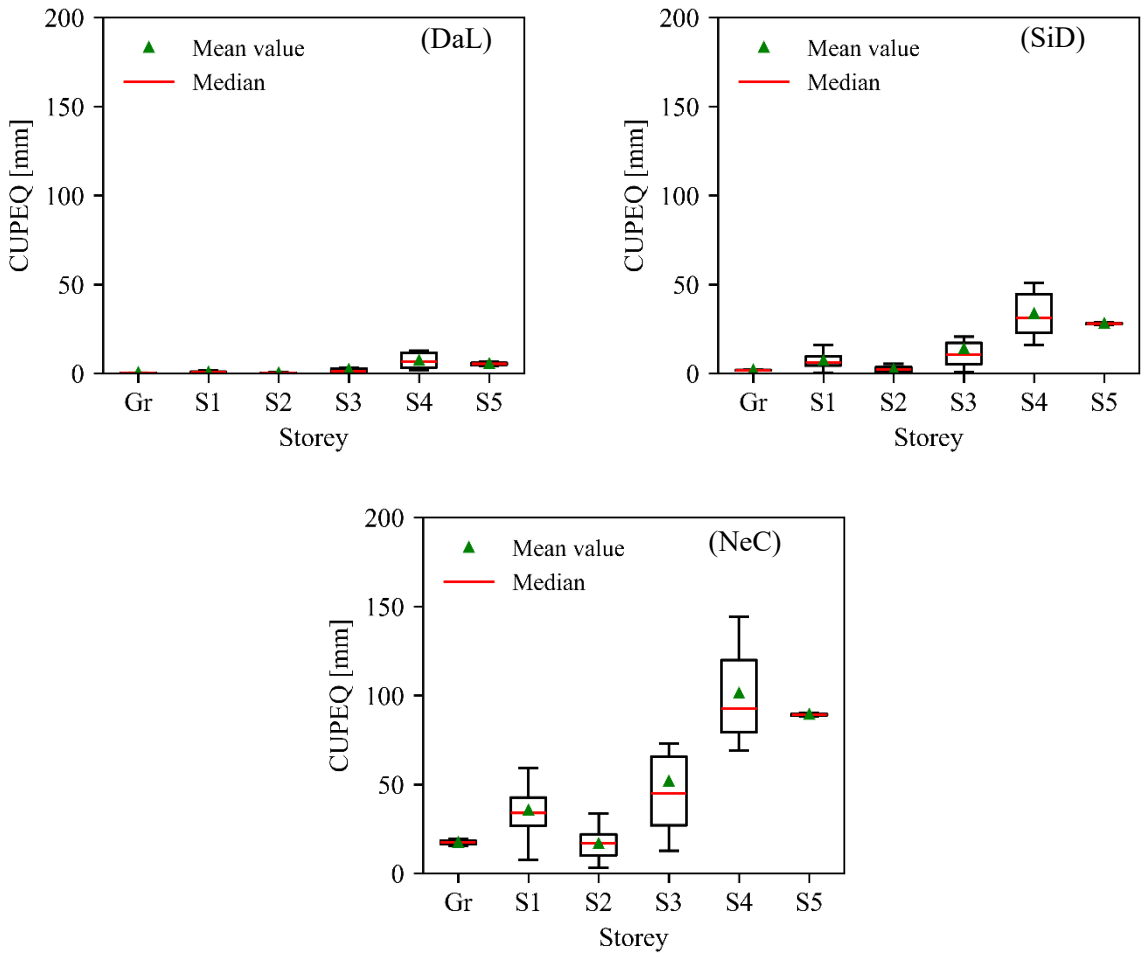

Fig. 7: CUPEQ distribution of connectors under EQ5 at DaL level, SiD level, and NeC level.

At the local level, the spider arm connectors exhibited pronounced nonlinearity, with CUPEC increasing significantly with increasing seismic intensity. The statistical evaluation across multiple ground motions confirmed that upper-storey connectors are particularly susceptible to damage. A reference CUPEC threshold based on the connector yielding displacement was adopted. The results show that, using a yielding-based CUPEC threshold, some connectors exceed it under DaL, while most exceed it under SiD and NeC, reflecting plastic behaviour. The finding underlines the importance of explicitly modelling PFGFS and their connectors in seismic assessments and suggests that current design practices may underestimate façade vulnerability. Future research should be focused on experimental validation and the development of simplified amplification factors for practical design applications.

Acknowledgements

The first author acknowledges the partial funding provided by the Portuguese Foundation for Science and Technology (FCT) through the doctoral grant 2023.01791.BD, (https://doi.org/10.54499/2023.01791.BD) through national funds (PIDDAC), under R2UTechnologies – Modular system (Ref. C644876810-00000019), supported by the Recovery and Resilience Plan (PRR), under the R&D Unit Institute for Sustainability and Innovation in Structural Engineering (ISISE), with references UID/4029/2025 (https://doi.org/10.54499/UID/04029/2025) and UID/PRR/04029/2025 (https://doi.org/10.54499/UID/PRR/04029/2025), and under the Associate Laboratory Advanced

Production and Intelligent Systems ARISE with reference LA/P/0112/2020. Additional funding was provided by FCT under the project POCI-01-0145-FEDER-032539 (GF-Seismic – Structural Glass Façades Subjected to Seismic Load).

References

Baird, A., Palermo, A., & Pampanin, S. (2011). Facade damage assessment of multi-storey buildings in the 2011 Christchurch earthquake. Bulletin of the New Zealand Society for Earthquake Engineering, 44(4), Article 4. https://doi.org/10.5459/bnzsee.44.4.368-376

Baird, A., Tasligedik, A. S., Palermo, A., & Pampanin, S. (2014). Seismic performance of vertical nonstructural components in the 22 February 2011 Christchurch earthquake. Earthquake Spectra, 30(1), 401–425.

Bedon, C., Zhang, X., Santos, F., Honfi, D., Kozłowski, M., Arrigoni, M., Figuli, L., & Lange, D. (2018). Performance of structural glass facades under extreme loads – Design methods, existing research, current issues and trends. Construction and Building Materials, 163, 921–937. https://doi.org/10.1016/j.conbuildmat.2017.12.153

Behr, R. A., Belarbi, A., & Brown, A. T. (1995). Seismic performance of architectural glass in a storefront wall system. Earthquake Spectra, 11(3), 367–391.

Code, P. (2014). Guidance for European Structural Design of Glass Components. Brussels: European Committee for Standardisation, 2014.

EN 1998-5, "Eurocode 8: Design of structures for earthquake resistance – Part 5: Foundations, retaining structures and geotechnical aspects", European Committee for the Standardisation, Brussels, 2004.

FEMA E-74—Reducing the Risks of Nonstructural Earthquake Damage – A Practical Guide. (2012).

Fierro, E. A., Miranda, E., & Perry, C. L. (2011). Behavior of Nonstructural Components in Recent Earthquakes. AEI 2011, 369–377. https://doi.org/10.1061/41168(399)44

Filiatrault, A., Uang, C.-M., Folz, B., Chrstopoulos, C., & Gatto, K. (2001). Reconnaissance report of the February 28, 2001 Nisqually (Seattle-Olympia) earthquake (SSRP–2001/02). Department of Structural Engineering, University of California.

Hosseini, M. (2005). Behavior of nonstructural elements in the 2003 Bam, Iran, earthquake. Earthquake Spectra, 21(1_suppl), 439–453.

Hosseini, S. A., Jordão, S., Bedon, C., & Rebelo, C. (2025). Seismic Floor Acceleration Demands for European Steel Frames Designed with Different Damage Limitation Criteria. In Á. Cunha & E. Caetano (Eds), Experimental Vibration Analysis for Civil Engineering Structures (Vol. 676, pp. 663–671). Springer Nature Switzerland. https://doi.org/10.1007/978-3-031-96114-4_68

Hosseini, S. A., Jordão, S., Rebelo, C., & Bedon, C. (2022). Control devises to reduce the seismic vibration of glass façade systems: A review. JPEE2022, Lisbon, Portugal.

Hosseini, S. A., Jordão, S., Rebelo, C., & Bedon, C. (2024). Impact of fragile nonstructural elements on the cost-effective seismic design of steel MRFs. SÍSMICA 2024, Guimarães, Portugal.

Inca-Cabrera, E., Jordão, S., Rebelo, C., Bedon, C., Mesquita, A., & Hosseini, S.-A. (2025). Experimental and numerical investigation of in-plane cyclic response of a point-fixed glass façade system for seismic performance assessment. Journal of Building Engineering, 108, 112956. https://doi.org/10.1016/j.jobe.2025.112956

Miranda, E., Mosqueda, G., Retamales, R., & Pekcan, G. (2012). Performance of nonstructural components during the 27 February 2010 Chile earthquake. Earthquake Spectra, 28(1_suppl1), 453–471.

Pantelides, C., Truman, K., Behr, R., & Belarbi, A. (1996). Development of a loading history for seismic testing of architectural glass in a shop-front wall system. Engineering Structures, 18(12), 917–935.

PEER Ground Motion Database - PEER Center, https://ngawest2.berkeley.edu/

Sivanerupan, S., Wilson, J., Gad, E., & Lam, N. (2014). Drift performance of point fixed glass façade systems. Advances in Structural Engineering, 17(10), 1481–1495.

Takeuchi, T., Yasuda, K., & Iwata, M. (2006). Studies on integrated building façade engineering with high-performance structural elements. 92, 33–40.

Takeuchi, T., Yasuda, K., & Iwata, M. (2009). Seismic retrofitting using energy dissipation façades. In Improving the Seismic Performance of Existing Buildings and Other Structures (pp. 1000–1009).

Challenging Glass Conference Proceedings – Volume 10 – June 2026 – Louter, Bos & Belis (Eds.)
International Conference on the Architectural and Structural Application of Glass
Challenging Glass Conference 10 – 15-17 June 2026 – TU Delft – The Netherlands

Platinum Sponsor

SAINT-GOBAIN

Gold Sponsors

EASTMAN

kuraray

NorthGlass®

sedak

seele

Silver Sponsors

DOW®

octatube

PERMASTEELISA GROUP

SEEN

Organisation

TU Delft

Technische Universität München

GHENT UNIVERSITY